Available online at www.eccomasproceedia.org
Eccomas Proceedia COMPDYN (2025) 805-817

ECCOMAS
Proceedia

COMPDYN 2025
10th ECCOMAS Thematic Conference on
Computational Methods in Structural Dynamics and Earthquake Engineering
M. Papadrakakis, M. Fragiadakis (eds.)
Rhodes Island, Greece, 15-18 June 2025

PREDICTING AND VALIDATING BUILDING RESPONSE TO INDUCED SEISMICITY FROM GEOTHERMAL OPERATIONS

Sonja Cebulj[1], Francesca Taddei[1], and Gerhard Müller[1]

[1]Chair of Structural Mechanics,Technical University of Munich (TUM)
Arcisstr. 21, 80333, Munich, Germany
e-mail: {sonja.cebulj, francesca.taddei, gerhard.mueller}@tum.de

Abstract. *Geothermal energy holds significant potential as a carbon-neutral energy source. However, one major challenge is the risk of induced seismicity during its operation. Given the proximity of geothermal power plants to populated areas, even minor seismic events might be felt by residents and raise substantial public concern. Assessing the risk for the serviceability of existing buildings and infrastructure near geothermal power plants is crucial, particularly around the injection well endpoint. This study aims to validate the prediction of building response using newly developed Ground Motion Prediction Equations (GMPEs) through comparison with experimental data. To achieve this, continuous monitoring was conducted on a low-rise office building in the Munich area, Germany, recording both minor environmental and usage-related vibrations, as well as a brief sequence of geothermal-induced seismic events. Furthermore, free-field motion data from the local seismic network was utilised to characterize the seismic events in greater detail. The building response prediction is generated using a finite element (FEM) model combined with a multi-modal response spectrum analysis. The comparison is conducted regarding velocity, evaluated separately for the vertical and horizontal directions.*

Keywords: Induced seismicity, Geothermal energy, Seismic monitoring

ISSN:2623-3347
Peer-review under responsibility of the organizing committee of COMPDYN 2025.
doi: 10.7712/120125.12448.25341

1 Introduction

Deep geothermal energy represents an alternative energy supply independent of the use of fossil resources. The great advantage of geothermal energy is its availability independent of the time of day, seasonal changes and weather conditions. The Greater Munich Area has favorable conditions for geothermal energy production because it is part of the Bavarian Molasse Basin and has a deep aquifer with high temperatures and high flow rates. Although the region is almost seismically inactive, there have been reported earthquakes associated with geothermal power plants [1]. Geothermal-induced events are generally minor in terms of magnitude, but they may still be noticeable due to their proximity to inhabited areas. This proximity is a consequence of the location of geothermal energy producers close to the consumers in order to avoid long transportation distances [2]. As part of the infrastructure, geothermal energy is subject to serviceability requirements similar to other continuously used infrastructure. Serviceability issues can also cause economic damage due to the limitation of geothermal power plants. Therefore, a scientific analysis of the induced seismicity and its effects on buildings and humans is necessary [3]. As the knowledge about induced seismicity in the Greater Munich Area is still very limited, a numerical simulation of induced events is performed in the work of Keil et al. [1] using the example of the geothermal power plant Poing, which is also located in the Munich area. These simulations together with recorded seismic data are used by Taddei et al. [4] in a statistical analysis to generate ground motion prediction equations for the considered areas. However, for the interface between the soil and the building, separate models are required that take into account the soil-structure interaction. Kumawat et al. [5] solve this soil-structure interaction using lumped-parameter models that simulate the behavior of the soil through mass-damper-spring systems. Taddei et al. [6] instead use an approach in which the soil is implemented by the boundary element method (BEM) and the structure is implemented by the finite element method (FEM), and subsequently the two domains are coupled. In order to complement the simulation data with real data, a monitoring system was installed in 2023 in several buildings close to geothermal power plants in the Munich area. Altough in the past seismicity was quite rare, two events could be recorded in November in Taufkirchen. These events were also recorded by BayernNetz, a network of 30 digital seismic stations designed for monitoring the seismic activity in Bavaria and neighbouring areas. Besides the monitoring system, the building was provided with supplementary accelerometers and subjected to an artificial impulse to gain a more detailed understanding of the functionality of the structure.
The measurement campaign is outlined in chapter 2 and the recorded data are presented in chapter 3. Chapter 4 describes the validation of the builiding response prediction by the combination of ground motion prediction equations and the finite element model against the recorded data.

2 Measurement campaign

The measurement campaign involves several data sources. First, the vibrational long-term monitoring of a building is presented in section 2.1. Section 2.2 describes the vibration analysis of the building perfomed by installing further sensors and exciting the building artificially by a falling weight and a hammer. The data network delivering the general seismic data is introduced in section 2.3.

2.1 Long-term monitoring

The long-term monitoring was conducted in an office building, which is adjacent to a geothermal power plant. The building has a triangular shape with dimensions of 9 m by 9 m and con-

sists of three levels: ground, first and second floor. The building has no basement, so the ground floor is based on the foundation. Figure 1 shows the layout of the building. For the long-term monitoring, one geophone was installed on each floor of the building, the locations of which are marked in the floor plans. The building was in use during the monitoring period, so the locations of the geophones were adapted to suit the usage of the building. Therefore the geophone in the ground floor was located in the technic room located in the adjacent structure. The time-synchronised wireless measurement network comprises geophones with a measurement range of ± 200 mm/s and an orthogonal, triaxial topology [7]. Continuous monitoring was conducted between June 2023 and April 2024.

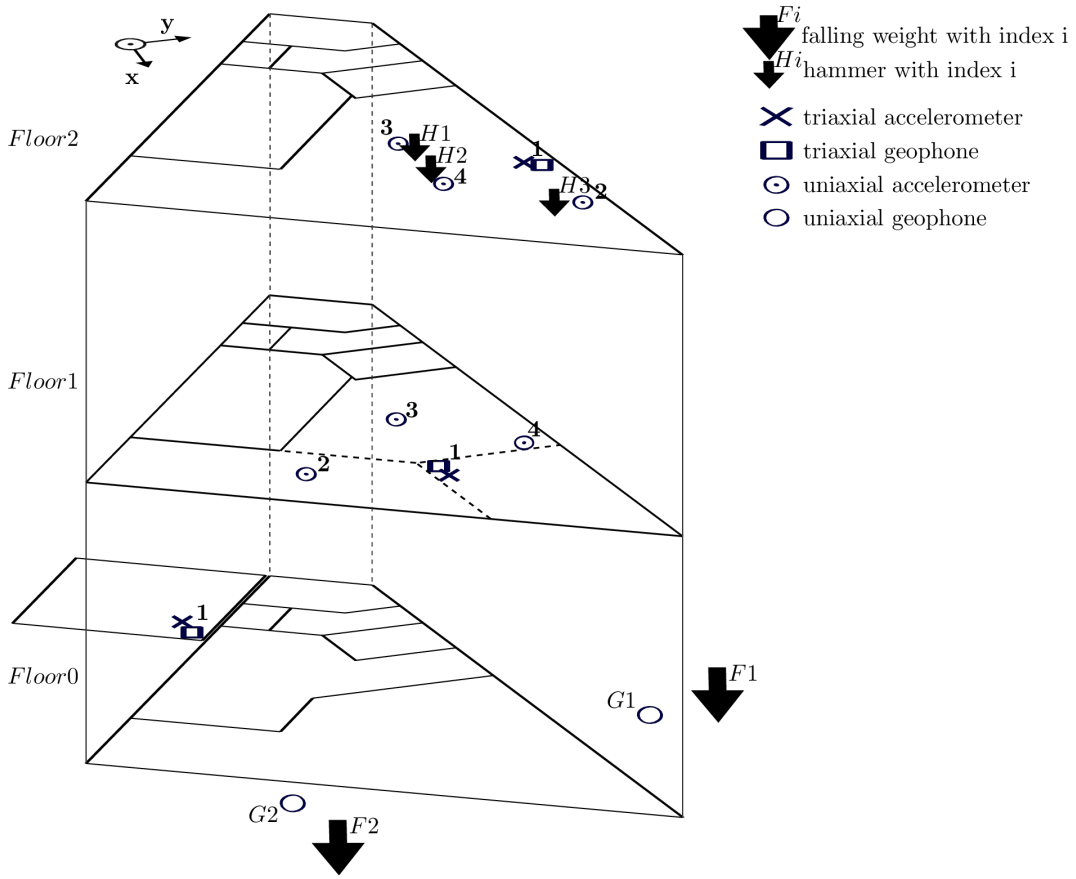

Figure 1: Building structure indicating shape and floors of the building and the locations of geophones, accelerometers and designed load scenarios.

2.2 Vibration analysis using designed load scenarios

To further refine the monitoring data, the geophone measurement of the induced seismic events is supplemented by accelerometers and artificial load scenarios. Regarding the accelerometers, triaxial sensors were installed adjacent to the geophones of the long-term monitoring for validation purposes. In addition, uniaxial sensors were installed at different locations on the slabs and the walls. The triaxial sensors utilised in this study are PCB sensors of type 256B18, with a nominal sensitivity of 1000 mV/g and a frequency range of 0.5 Hz - 3 kHz. The uniaxial sensors located on the slab are B&K sensors of type 4514002 with a nominal sensitivity of 500 mV/g and a frequency range of 1 Hz - 10 kHz. Two uniaxial B&K sensors with a

nominal sensitivity of 100 mV/g and a frequency range of 1 Hz - 10 kHz were located on the walls.

In order to excite the first eigenmodes of the slabs, the objective is to generate low-frequency excitations, primarily below 40 Hz. These low-frequent vibrations are also of particular interest in the context of serviceability, as the threshold of perception in terms of amplitude are lower at low frequencies than at high frequencies. Therefore, the falling weight method was selected for the experiment, with a 650 kg steel cylinder serving as the mass. This cylinder was suspended by an electromagnetic module and released through the deactivation of the electromagnetic field. The falling weight dropped at the parking area at a distance of approximately 8 m from the building. As the road surface should not be destroyed, the weight was dropped on a wooden plank from a height of 1.5 m.

In order to conduct local tests and a modal analysis, hammer measurements were taken. The impulse hammer test was carried out using an impulse force hammer PCB 086D50. The hammer mass is 5.5 kg and the resonant frequency of the hammer is above 5 kHz. This hammer was chosen over lighter and smaller options in order to extend the impact amptlitude and induce sufficient vibrations for the first and second floor. The hammer tests were conducted at the second floor, applying several sets of impacts at different locations of the slab in the second floor. The different locations of the falling weight and hammer load scenarios are marked in Figure 1.

2.3 Seismic network

The seismic activity in Bavaria is monitored by a network of 30 seismic stations (BayernNetz). The seismological branch of the Geophysical Observatory Fürstenfeldbruck by the Department for Earth and Environmental Sciences at Ludwig-Maximilians-University Munich forms the data and analysis center for BayernNetz. The data is accessed by FDSN Web Services [8].

3 Measurement results

First, the results of the monitoring for the seismic events that occured in November 2023 are presented in section 3.1. A comparison of the results of first and second floor showed that the data of the second floor is of higher quality. Additionally according to DIN 4150-3 [9] the velocities in the uppermost ceiling level are decisive for the assessment. Therefore the following analysis will focus on the results in the ground and second floor.

In the following section 3.2, the results of the vibration analysis of the designed load scenarios, namely the falling weight and the hammer test, are presented. For these scenarios, the building response was recorded by the accelerometers and the geophones.

3.1 Monitoring

The geophones that were installed for the continuous monitoring recorded slab oscillations triggerd by diverse environmental influences such as construction sites or usage of the building. However, in November 2023 four minor seismic events were recorded. Three of them occurred on 29.11.2023 with a magnitude of 1.3, 1.6 and 1.8 and one occurred on 20.11.2023 with a magnitude of 1.4. Table 1 provides an overview of the occurrence dates and times of the events, along with the respective magnitude, epicentral distance, and hypocentral distance. These events were identified as seismic events as they were also recorded by numerous stations of the network of seismic stations *BayernNetz* and occurred at a distance of about 3 km from the

event number	date	time	local magnitude	epicentral dist.	hypocentral dist.
Event 1	20.11.2023	05:31	1.4	2.97 km	4.22 km
Event 2	29.11.2023	09:32	1.3	3.17 km	4.36 km
Event 3	29.11.2023	12:38	1.8	3.28 km	4.45 km
Event 4	29.11.2023	13:01	1.6	3.28 km	4.45 km

Table 1: Internal event number, date, time, local magnitude, epicentral distance and hypocentral distance of the recorded seismic events

building. The map in Figure 2 provides the location of the geothermal power plant (GPP) and the occurence locations of the events. The information on the events was provided by the Bavarian Seismological Service. Figure 3 shows the building's response to the seismic excitation,

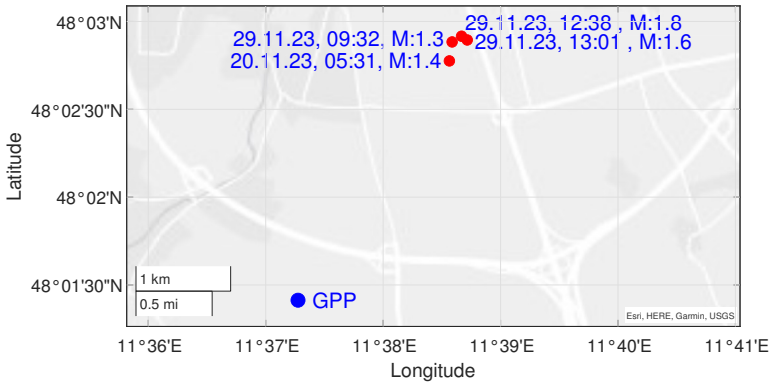

Figure 2: Map indicating the locations of the geothermal power plant and the epicenters of the induced events.

as recorded by the geophone on the second floor, in terms of velocities in time domain. Red circles indicate the absolute maximum velocity for each event. The resulting frequency spectra in horizontal and vertical direction are illustrated in Figure 4 and 5 respectively. The upper plots of both figures depict the velocities of the ground and second floor in third octave bands, while the lower plots illustrate the transfer functions from ground to second floor. In vertical direction, the third octave bands show a clear peak of velocities in the second floor at 12.5 Hz. The transfer function reflects this peak as a slight amplification compared to the ground floor. The rising transfer functions for higher frequencies are slightly amplified as the frequency bands get larger and cover more modes per band. In the horizontal direction, the velocities at the second floor and their transfer functions with respect to the ground floor show a significant increase at 5-6 Hz. As can be seen here, the observed peak frequencies are equal to those observed for the impulse hammer excitation. However it is also evident, that the absolute response of the slabs is higher in horizontal than in vertical direction. In both vertical and horizontal directions, the amplification from ground to the second floor reaches a maximum of 17 dB, occurring in the horizontal direction. The KB_{Fmax} values according to the approximation method of the German standard DIN 4150-3 [9] , are below 0.2, which corresponds to the limit for high comfort for storey ceilings in residential and industrial buildings. Only for the event 3 with a magnitude of 1.8 the KB_{Fmax} value reaches 0.255, which is still below the maximum value of 3 defined in the standard.

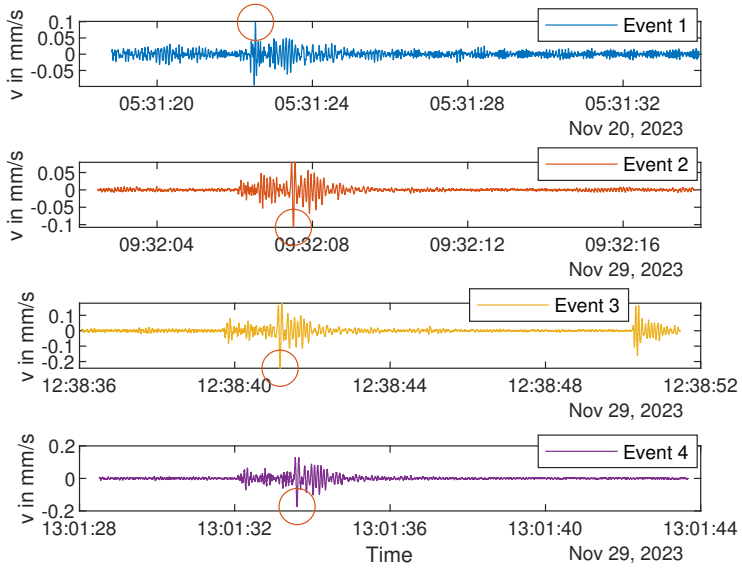

Figure 3: Building response to the induced seismic events recorded by the geophone on the second floor in terms of velocity in vertical direction in the time domain. Red circles mark the absolute maximum.

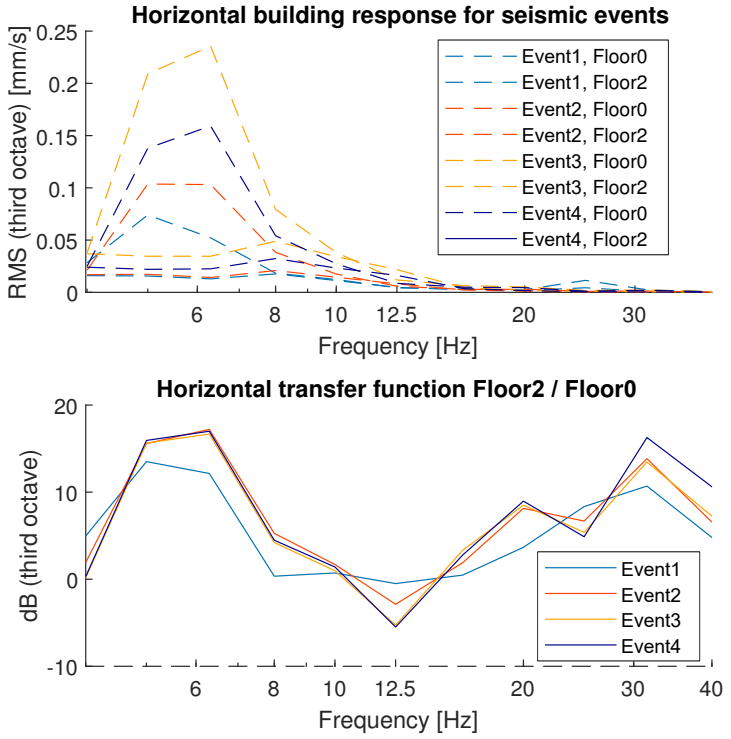

Figure 4: Horizontal amplitudes (y-direction) for induced seismic events: Top: third octave spectra. Bottom: transfer functions with respect to single measurement points.

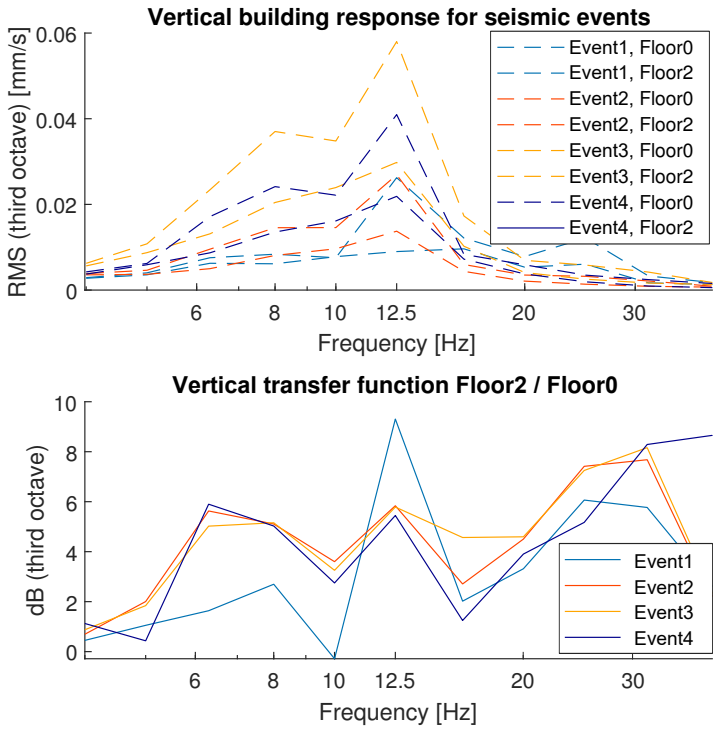

Figure 5: Vertical amplitudes for induced seismic events: Top: third octave spectra. Bottom: transfer functions with respect to single measurement points.

3.2 Vibration analysis

Figure 6 shows the velocity of the slab in the second floor generated by a impulse hammer according to section 2.2. The displayed velocities in horizontal and vertical direction were measured by the geophones that also recorded the seismic events and the falling weight excitation. The upper two plots display the velocity in horizontal direction, while the last plot presents the velocity in vertical direction. The locations $H1$, $H2$ and $H3$ are marked in Figure 1 and the indice _01 - _06 refer to the sequential hammer impacts at one location. The data from the accelerometers aditionally installed on the slabs show a good matching with the results of the geophones. In vertical direction, the peaks of the curves at 12 Hz and 20 Hz indicate the dominant frequency of the slab for a hammer excitation in vertical direction (z-direction). However, in horizontal direction (x-y-direction), the peak is less pronounced and occurs at lower frequencies of around 5-6 Hz. Furthermore, the absolute velocities are comparatively lower, due to the fact that the hammer excites mainly in vertical direction (z-direction). The falling weight excitation was implemented according to section 2.2. Figure 7 shows the horizontal building response in frequency domain for the second floor and the geophone location outside the building (see 1). The upper plot refers to the x-direction and the lower plot refers to the y-direction (see x- and y-direction in 1). Figure 8 shows the vertical building response in frequency domain for different falling weight excitations. The upper plot shows the velocities at the second floor and the geophone outside the building (see 1) and the lower plot shows the transfer functions from the geophone outside the building to the second floor according to [10]. In both Figures 7 and 8 the different colours mark the different load scenarios variing in the location of the impact. The locations $F1$ and $F2$ are marked in Figure 1 and the indice _01 - _04 refer to the sequential falling weight impacts at one location. For better comparability, the data are averaged over

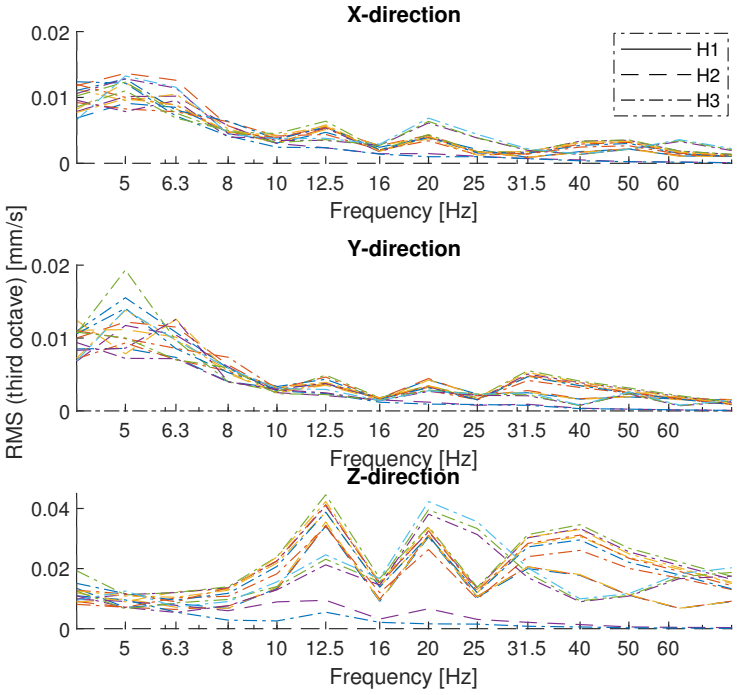

Figure 6: Amplitudes for hammer excitation. Third octave spectra in x-, y-, and z-direction. The different line styles indicate the locations $H1$, $H2$ and $H3$ according to Figure 1. The indices _01 - _06 refer to the sequential hammer impacts at the respective location $H1$, $H2$ or $H3$ and are represented by different colours.

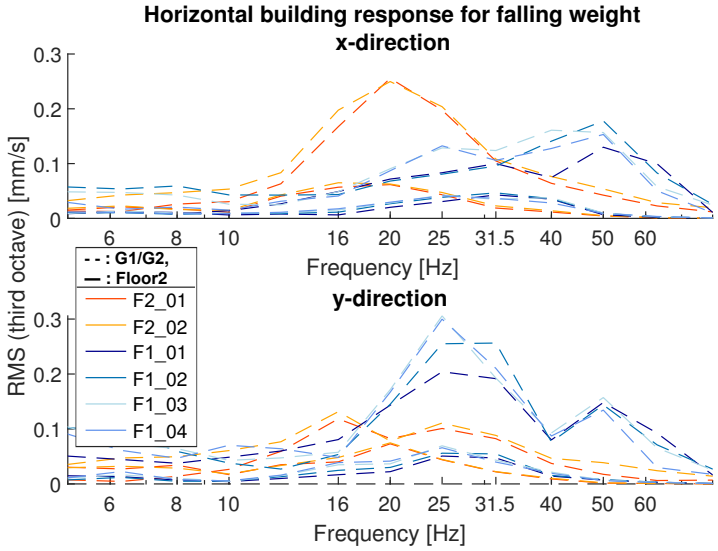

Figure 7: Horizontal amplitudes for falling weight excitation: Top: third octave spectra x-direction. Bottom: third octave spectra y-direction. The locations $F1$, $F2$, $G1$ and $G2$ are marked in Figure 1 and the indice _01 - _04 refer to the sequential falling weight impacts at the respective location $F1$ or $F2$.

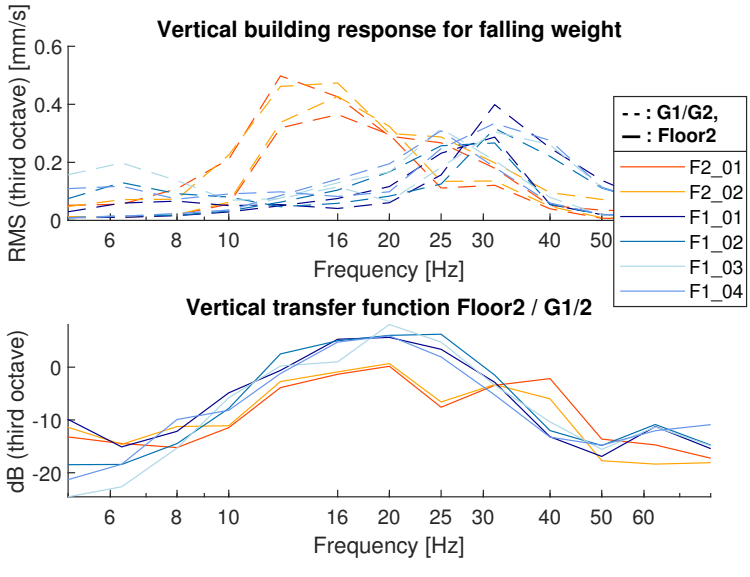

Figure 8: Vertical amplitudes for falling weight excitation: Top: third octave spectra. Bottom: transfer functions. The locations $F1$, $F2$, $G1$ and $G2$ are marked in Figure 1 and the indice _01 - _04 refer to the sequential falling weight impacts at the respective location $F1$ or $F2$.

third octave bands. The third octave bands of the second floor data show peaks at 16 Hz for the falling weight at location F2 and at 31.5 Hz for the falling weight at location F1. The transfer functions, however, show peaks in the range of 16 to 20 Hz. It should also be noted that the transfer functions in dB-scale are predominantly negative and must be considered qualitatively, given that the result refers to the geophone close to the drop weight. The results in the x- and y-direction (Figure 7) show an even poorer transfer of the drop weight excitation into the building. A representative transfer of horizontal vibrations into the building with the drop weight was thus not achieved.

A comparison of the locations F2 and F1 reveals that the drop weight at location F2 produces lower peak frequencies (12.5-16 Hz) than the drop weight at location F1 (31.5 Hz). In both cases, the drop weight was placed on a wooden plank. In the location F1 case, the plank was placed on the green area and in the location F2 case directly on the asphalt. These modified impact situations act as dynamic intermediate systems, influencing the spectrum of the impulse excitation.

4 Application of ground motion prediction equations

As a preliminary step, the building under consideration is implemented as a finite element (FE) model in Ansys. The building material of the considered building is concrete, resulting in a density of 2500 kg/m^3 and a Young's modulus of 30000 N/mm^2.

The soil-structure interaction between the soil and the FE model is solved through the implementation of a lumped parameter model attached to the footings according to [5]. The parameters utilised in these models are selected to represent the soil conditions prevalent in the Greater Munich Area. According to Keil et al. [1], the soil can be classified as stiff soil with a $V_{s,30}$ of 450 m/s and a densitiy of 2300 kg/m^3. With this model, a modal analysis is conducted, determining the vibration characteristics of the model. In a subsequent step, the ground motion prediction equations (GMPEs) newly developed for the considered area by Taddei et al. [4] are introduced. These GMPEs are empirical or semi-empirical spectral ground motion models

predicting seismic quantities as a function of several seismicity-related variables. This study focuses on the following GMPE [4]:

$$\begin{aligned} \log(Y) &= \beta_1 + \beta_2 M_W + \beta_3 lor(r) + \varepsilon \\ \text{with} \qquad & r = \sqrt{r_{hyp}^2 + h_{eff}^2} \\ \text{and} \qquad & h_{eff} = \max(0.5, 10^{(-0.28+0.19M_W)}), \end{aligned} \tag{1}$$

where β_1, β_2, and β_3 denote model parameters, ε is an error term and M_W and r are the model inputs denoting magnitude and radius. The design of this GMPE incorporates both redorded seismic data from Insheim and the Greater Munich Area as well as simulated data derived from physics-based simulations. The considered GMPE provides peak quantities, spectral accelerations and velocities, utilising the magnitude M_W and the radius r_{hyp} as input variables. The coefficients β_1 to β_3 applied in this study are documented in Taddei et al. [4]. The GMPE is then applied to the studied building location, with the input variables selected according to the site conditions of the four natural earthquakes on 20.11.2023 and 29.11.2023. The variables M_W and r_{hyp} are selected according to Table 1. The resulting response spectra in vertical direction are presented in Figure 9 and can be interpreted as the response of a series of oscillators to the seismic excitation.

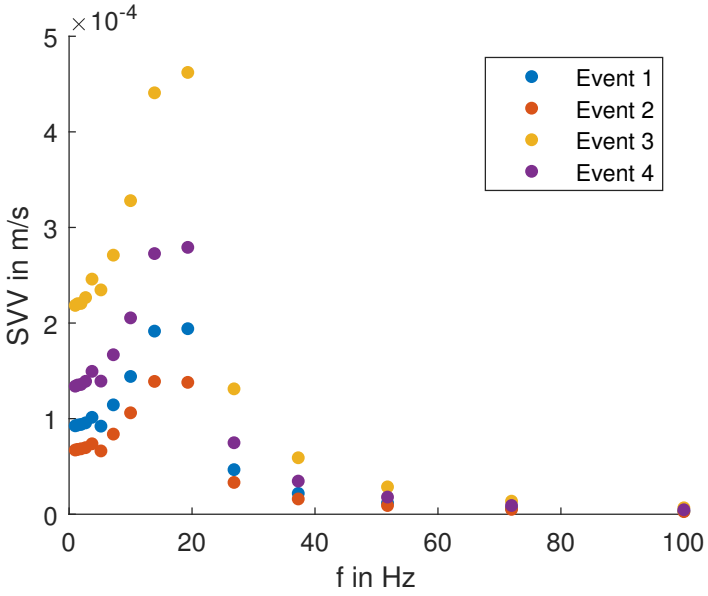

Figure 9: Spectral velocities in vertical direction, predicted by GMPEs for the Greater Munich Area for four different magnitudes.

Finally, these spectral velocities are used in combination with the modal analysis of the previously described FE model of the considered building, for a multimodal response spectrum analysis using the first 3 modes and a damping ratio of 0.05. To take into account the closely-spaced natural frequencies in vertical direction the modal superposition is performed using a complete quadratic mode combination method according to Wilson et al. [11]. Figure 10 illustrates the FE model with the simulated velocities resulting from the modal superposition. To facilitate a comparison with the recorded values, the nodal solution for the node corresponding to the geophone location on the second floor is generated. Figure 11 shows these simulated

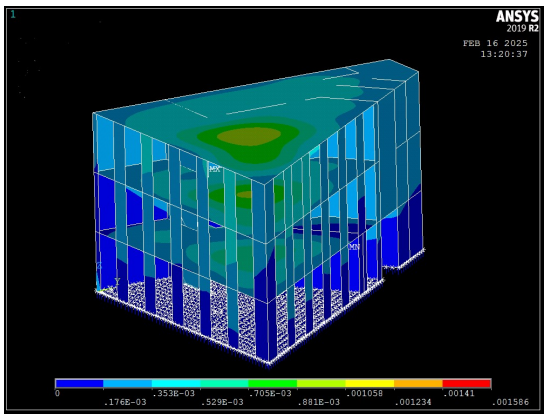

Figure 10: Finite element model predicting vertical velocities resulting from induced seismic events.

velocities at the sensor location (x), the recorded velocity at the sensor location (o) and the simulated velocity at the node with the maximal velocity occurring at the second floor (*), all of them in dependency of the respective event magnitude. The simulated vertical velocities are slightly higher than the recorded velocities, however both data show a good agreement. The difference between simulated and recorded data increases with increasing magnitude.

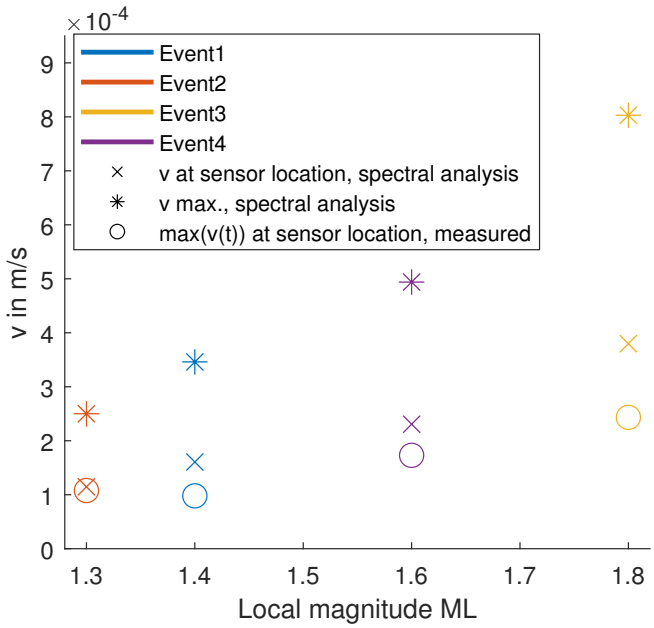

Figure 11: Comparison of the predicted vertical building response, the recorded vertical building response at the sensor location and the predicted maximum velocity on the second floor. All velocities are plotted in relation to the magnitude of the respective event.

5 Conclusion and Outlook

Geothermal power plants providing time and weather independet energy play an important role in the supply of renewable energy. However, they are associated with the risk of induced

seismicity, which can result in serviceability and comfort problems in nearby buildings. In order to assess this risk, a seismic long-term monitoring campaign was conducted at a geothermal power plant. The results of this campaign are presented in the first part of this paper. The experimental data is used to validate the prediction of the building response using newly developed GMPEs. Therefore the response spectra of the GMPEs are combined with a multi-modal response spectrum analysis of the monitored building resulting in a prediction for the building response. This building response prediction is very close to the recorded data of four induced seismic events, thus proving the applicability of the GMPEs for the studied area. By conducting more measurements, this validation can be extended to different building types establishing the foundation of a detailed risk assessment focusing on the building response prediction. This will enable the development of risk maps for areas with geothermal potential.

REFERENCES

[1] Keil, S., Wassermann, J., Megies, T., Estimation of ground motion due to induced seismicity at a geothermal power plant near Munich, Germany, using numerical simulations *Geothermics*, **106**, 102577, 2022

[2] G. Grünthal, Induced seismicity related to geothermal projects versus natural tectonic earthquakes and other types of induced seismic events in central europe *Geothermics*, **52**, 22–35, 2014

[3] A. Khansefid, S. M. Yadollahi, G. Müller, F. Taddei, and A. Kumawat, Seismic performance assessment of a masonry building under earthquakes induced by geothermal power plants operation, *Journal of Building Engineering* **48**, 103909, 2022.

[4] Taddei, F., Keil, S., Khansefid, A. et al. , Development and Use of Semi-empirical Spectral Ground Motion Models for GPP-Induced Micro-earthquakes in Southern Germany *Bulletin of Earthquake Engineering*, **22**, 5403–5450, 2024

[5] Kumawat, A. ; Taddei, F. ; Csuka, A. ; Cudmani, R. ; Müller, G., Response analysis of low-rise buildings under micro seismic events induced by geothermal operations *International Conference on Noise and Vibration Engineering (ISMA)*, 2022

[6] Taddei, F. ; Chocholaty, B. ; Müller, G., Time Domain BEMFEM Coupling for Seismic Soil-Structure Interaction Analyses Conceived for an AnsysMatlab Workflow *International Conference on Structural Dynamics (EURODYN 2020)*, 2985–3004, 2020

[7] SEMEX-EngCon GmbH, Vibration measuring device MENHIR, Data sheet, available at: https://www.semex-engcon.com/en/measuring-equipment/menhir; Accessed: 20-February-2025

[8] FDSN and EIDA Web Services, Geophysical Observatory, Department of Earth and Environmental Sciences, Ludwig-Maximilians-Universität München, 2024, available at: https://www.geophysik.uni-muenchen.de; Accessed: 23-April-2024

[9] DIN 4150-3: Vibrations in buildings – Part 3: Effects on structures *Deutsches Institut für Normung e.V. (DIN)*, 2016

[10] H.G. Natke, Einführung in Theorie und Praxis der Zeitreihen und Modalanalyse *Springer Vieweg*, 1983

[11] Wilson, E. L., Der Kiureghian, A., Bayo, E., A replacement for the SRSS method in seismic analysis. *Earthquake Engineering & Structural Dynamics*, **9**, 187-192, 1981

ACKNOWLEDGEMENT

The authors gratefully acknowledge the funding through the joint research project Geothermal-Alliance Bavaria (GAB) by the Bavarian State Ministry of Science and the Arts.